Quantifying Antivascular Effects of Monoclonal Antibodies to Vascular Endothelial Growth Factor: Insights from Imaging

James P.B. O'Connor,[1,2] Richard A.D. Carano,[3] Andrew R. Clamp,[2] Jed Ross,[3] Calvin C.K. Ho,[3] Alan Jackson,[1] Geoff J.M. Parker,[1] Chris J. Rose,[1] Franklin V. Peale,[4] Michel Friesenhahn,[5] Claire L. Mitchell,[1,2] Yvonne Watson,[1] Caleb Roberts,[1] Lynn Hope,[2] Sue Cheung,[1] Hani Bou Reslan,[3] Mary Ann T. Go,[6] Glenn J. Pacheco,[6] Xiumin Wu,[7] Tim C. Cao,[3] Sarajane Ross,[6] Giovanni A. Buonaccorsi,[1] Karen Davies,[1] Jurjees Hasan,[2] Paula Thornton,[2] Olivia del Puerto,[8] Napoleone Ferrara,[7] Nicholas van Bruggen,[3] and Gordon C. Jayson[2]

Abstract

Purpose: Little is known concerning the onset, duration, and magnitude of direct therapeutic effects of anti–vascular endothelial growth factor (VEGF) therapies. Such knowledge would help guide the rational development of targeted therapeutics from bench to bedside and optimize use of imaging technologies that quantify tumor function in early-phase clinical trials.

Experimental Design: Preclinical studies were done using *ex vivo* microcomputed tomography and *in vivo* ultrasound imaging to characterize tumor vasculature in a human HM-7 colorectal xenograft model treated with the anti-VEGF antibody G6-31. Clinical evaluation was by quantitative magnetic resonance imaging in 10 patients with metastatic colorectal cancer treated with bevacizumab.

Results: Microcomputed tomography experiments showed reduction in perfused vessels within 24 to 48 h of G6-31 drug administration ($P \leq 0.005$). Ultrasound imaging confirmed reduced tumor blood volume within the same time frame ($P = 0.048$). Consistent with the preclinical results, reductions in enhancing fraction and fractional plasma volume were detected in patient colorectal cancer metastases within 48 h after a single dose of bevacizumab that persisted throughout one cycle of therapy. These effects were followed by resolution of edema ($P = 0.0023$) and tumor shrinkage in 9 of 26 tumors at day 12.

Conclusion: These data suggest that VEGF-specific inhibition induces rapid structural and functional effects with downstream significant antitumor activity within one cycle of therapy. This finding has important implications for the design of early-phase clinical trials that incorporate physiologic imaging. The study shows how animal data help interpret clinical imaging data, an important step toward the validation of image biomarkers of tumor structure and function. (Clin Cancer Res 2009;15(21):6674–82)

Vascular endothelial growth factor (VEGF) plays a crucial role in angiogenesis by promoting endothelial cell proliferation, migration, and vascular permeability. These effects enable tumor growth and survival (1, 2). Consequently, VEGF signaling has become an important target in drug development and has led to Food and Drug Administration approval of drugs that target either VEGF or the VEGF receptor (3, 4). In particular, phase III trials of the humanized anti-VEGF monoclonal antibody bevacizumab (Avastin; Genentech) in combination with cytotoxic chemotherapeutics have shown improved overall survival in patients with metastatic colorectal cancer (CRC; ref. 5) and non–small cell lung cancer (6). Improved

Authors' Affiliations: [1]Imaging Science and Biomedical Engineering, School of Cancer and Imaging Sciences, University of Manchester and [2]Cancer Research UK and University of Manchester Department of Medical Oncology, Christie Hospital, Manchester, United Kingdom; [3]Biomedical Imaging Group, Department of Tumor Biology and Angiogenesis, Departments of [4]Pathology, [5]Biostatistics, [6]Translational Oncology and [7]Ferrara Laboratory, Genentech, Inc., South San Francisco, California; and [8]Roche Products Limited, Hertfordshire, United Kingdom

Received 3/26/09; revised 8/4/09; accepted 8/10/09; published OnlineFirst 10/27/09.

Grant support: Roche Products Ltd. and by Cancer Research UK grant C19221/A6086 (J.P.B. O'Connor).

The costs of publication of this article were defrayed in part by the payment of page charges. This article must therefore be hereby marked *advertisement* in accordance with 18 U.S.C. Section 1734 solely to indicate this fact.

Note: Supplementary data for this article are available at Clinical Cancer Research Online (http://clincancerres.aacrjournals.org/).

J.P.B. O'Connor, R.A.D. Carano, and A.R. Clamp contributed equally to this work.

Requests for reprints: James O'Connor, Imaging Science and Biomedical Engineering, School of Cancer and Imaging Sciences, University of Manchester, Oxford Road, Manchester, M13 9PT, United Kingdom. Phone: 44-161-275-0040; Fax: 44-161-275-0003; E-mail: james.o'connor@manchester.ac.uk.

doi:10.1158/1078-0432.CCR-09-0731

Translational Relevance

Dynamic contrast-enhanced magnetic resonance imaging (DCE-MRI) can provide pharmacodynamic biomarkers of drug effect in studies of antiangiogenic and antivascular agents. This technique is incorporated increasingly in early-phase clinical trials of novel therapeutic agents. In this study of bevacizumab, we report DCE-MRI data that enhances current understanding of the temporal evolution of direct effects induced by anti–vascular endothelial growth factor antibody therapy. In addition, we show how corroborative preclinical data can help distinguish between those DCE-MRI parameters that are sensitive to changes in tumor function and those that measure structure. These findings not only provide valuable insight into drug mechanism of action but also emphasize the need to optimize image timing and selection of analysis parameters when applying functional image techniques into clinical trials.

progression-free survival has also been reported in metastatic breast cancer (7).

These reports have led to rapid adoption of anti-VEGF therapies into clinical practice. This has been accompanied by interest in developing noninvasive image biomarkers that are sensitive to changes in the tumor microvasculature, because anti-VEGF therapies typically exhibit cytostatic rather than cytotoxic effects on tumor growth with little reduction in tumor size (8, 9). In particular, dynamic contrast-enhanced magnetic resonance imaging (DCE-MRI) has been incorporated in early-phase clinical trials of anti-VEGF antibody therapy (10, 11), tyrosine kinase inhibitors (TKI; refs. 12, 13) and vascular disrupting agents (VDA; ref. 14), to provide pharmacodynamic end points to assess drug activity.

At present, relatively little is known about the onset, magnitude, duration and temporal evolution of anti-VEGF therapy antivascular effects. Such information should have important implications for the rational development of targeted therapeutics and for the optimal design of future clinical trials incorporating physiologic imaging end points (15, 16). To explore this issue, we performed clinical studies to evaluate the effects of bevacizumab in CRC patients with liver metastases using DCE-MRI.

Corroborative data were provided from preclinical studies using X-ray microcomputed tomography (micro-CT) angiography, DCE ultrasound (DCE-US) and histology in a CRC murine HM-7 xenograft model. The HM-7 model was chosen because of the strong response (based on tumor size) of this tumor cell line to anti-VEGF therapy and with the goal to better understand the vascular effects of a highly responsive tumor. Preclinical studies were done with G6-31, a novel antibody to VEGF-A. G6-31 is a high-affinity antibody to both murine and human VEGF-A, which has ~10 times greater binding affinity to human VEGF than A4.6.1 or the humanized version (bevacizumab). G6-31 has been shown to provide greater efficacy in preclinical xenograft models (including HM-7) than bevacizumab due to its ability to bind both tumor (human) and stromal (mouse) VEGF (17).

The primary aim of this study was to define the temporal evolution of antivascular effects induced during a single cycle of anti-VEGF monotherapy. The secondary aim was to investigate whether cross-species imaging could provide insight into drug mechanism of action.

Materials and Methods

Preclinical studies

Animal preparation. The Genentech, Inc. Association for Assessment of Accreditation of Laboratory Animal Care-accredited review board approved all animal procedures. HM-7 human colon cancer cells (5×10^6 cells per animal) were implanted s.c. in the flanks of female athymic nude mice (Charles River Laboratory). Mice weighed between 20 to 25 grams. Tumors were grown to between 100 and 300 mm^3 (where volume = 0.5 × length × $width^2$) at which point animals were enrolled into study.

Micro-CT angiography time course study. Forty-one animals were randomized into two treatment groups. Animals received 5 mg/kg i.v. (90-min study) or i.p. (24- and 48-h studies) injection of either G6-31 or isotype control antibody. I.v. dosing was used for the 90-min study to maximize exposure over the 90 min of the experiment. Micro-CT angiography was used to measure vascular density in murine HM-7 xenografts, performed after animals were sacrificed at three time points: 90 min (G6-31, $n = 6$; control, $n = 6$), 24 h (G6-31, $n = 4$; control, $n = 4$), and 48 h (G6-31, $n = 10$; control, $n = 11$).

The micro-CT angiography methodology used in this study has been described previously in detail (18). In brief, animals were perfused with MICROFIL lead chromate latex immediately after sacrifice. The infused latex mixture was allowed to polymerize at room temperature for 60 min before tissue harvest. Dissected tumors were immersed in 10% neutral buffered formalin.

Tumors were then imaged with a μCT40 (SCANCO Medical) system (tube, 45 kV; current, 177 μA; integration time, 450 ms; isotropic resolution, 16 μm). An intensity threshold of 1,195 Hounsfield Units (HU) and morphologic filtering (erosion and dilation) were applied to the volumetric micro-CT image data to extract the vascular volume (VV). Tumor volume (TV) was extracted from the background in similar fashion with an intensity threshold of -8 Hounsfield Units. Vascular density was calculated as the ratio of vascular volume to TV. Vascular and tumor intensity thresholds were determined by visual inspection of the segmentation results from a separate set of samples. Computations were done by an in-house image analysis algorithm written in C++ and Python that used the AVW image processing software library (AnalyzeDirect, Inc.). Three-dimensional surface renderings were created from the micro-CT data with the use of Analyze 7.0 (AnalyzeDirect, Inc.).

Tumors were then evaluated by MECA-32 histology. Formalin-fixed, paraffin-embedded tissue sections were deparaffinized and pretreated with Target Retrieval (Dako) at 99°C for 20 min. Quenching of endogenous peroxidase activity and blocking of endogenous biotin (Vector) followed at room temperature. Sections were further blocked for 30 min with 10% normal rabbit serum in PBS with 3% bovine serum albumin. Tissue sections were then incubated with rat anti-mouse panendothelial cell antigen, clone MECA-32 at 2 μg/mL (BD Biosciences) for 60 min, biotinylated rabbit anti-rat at 2.5 μg/mL (Vector) for 30 min, ABC reagent (Vector) for 30 min, followed by a 5-min incubation in Metal Enhanced DAB (Pierce). Sections were counterstained with Mayer's hematoxylin. MECA-32–stained sections were analyzed with an Ariol SL-50 slide scanning platform (Applied Imaging), using a ×10 objective to quantify vascular density. Tumor regions were identified and outlined manually. Pixel colors corresponding to MECA-32 staining were defined using a customized Metamorph software (Molecular Devices) algorithm and vascular area was measured and normalized to tumor area.

DCE-US and micro-CT angiography study. Thirty-eight animals were randomized into two treatment groups, control and G6-31, as follows: 4 h (G6-31, $n = 13$; control, $n = 13$) and 48 h (G6-31, $n = 6$; control, $n = 6$). Pretreatment ultrasound imaging was done to measure TV. Animals

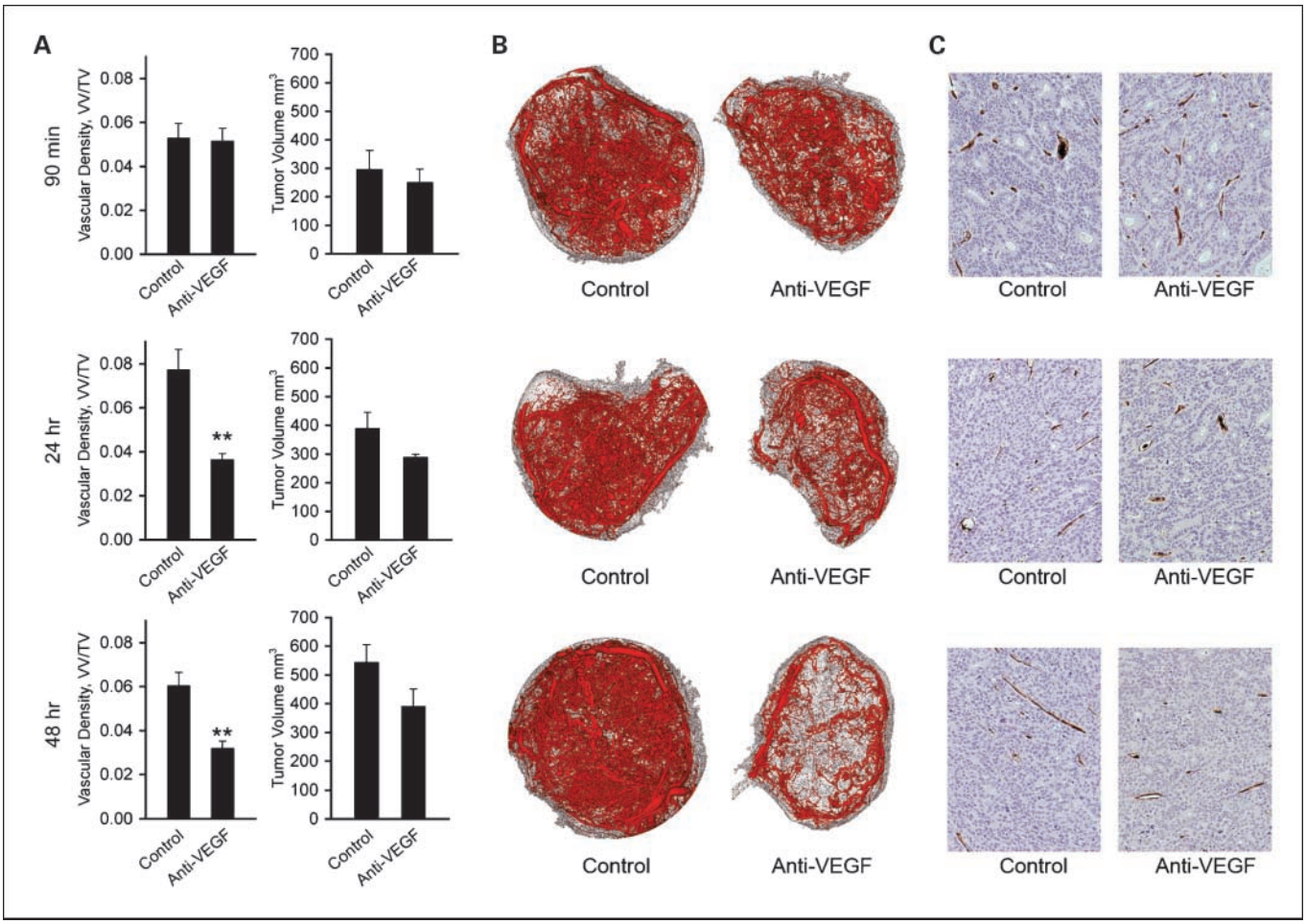

Fig. 1. *Ex vivo* evidence for rapid antivascular effects of G6-31. *A,* change in vascular density (*VV/TV*), as measured by micro-CT at 90 min, 24 h, and 48 h in control animals and those treated with the anti-VEGF antibody G6-31. *B,* representative micro-CT angiographic data for each treatment group at 90 min and at 24 and 48 h. Extracted vascular network (*red*) and entire tumor (*gray*) are shown. *C,* histologic sections stained with MECA-32 for corresponding time points. Note that the brown intravascular pigment is micro-CT lead chromate contrast agent, which only partially fills vessel lumens after histologic processing. Vessel area was measured by assessing 3,3′-diaminobenzidine–stained endothelium at the vessel perimeter. See Supplementary Fig. S1 for the corresponding segmented images.

then received 5 mg/kg i.v. (4-h study) or i.p. (48-h study) injection of either G6-31 or isotype control antibody. Intravenous dosing was used for the 4-h study to maximize exposure over the 4 h of the experiment. Ultrasound imaging was repeated 4 or 48 h posttreatment, after which animals were sacrificed and micro-CT angiography was done.

Mice were anesthetized using 2% isoflurane delivered in medical air at 1 L/s flow rate and placed supine on a dedicated small animal holding system (VisualSonics, Inc.). Temperature was maintained at 37°C with a heated imaging platform. Body temperature and heart rate were monitored (THM 150, Indus Instruments). Imaging was done with a Vevo 770 micro-imaging system (VisualSonics, Inc.) using a single-element ultrasound transducer (center frequency, 40 MHz; focal length, 6 mm; axial resolution, 40 μm; lateral resolution, 100 μm).

Microbubble ultrasound contrast agent (Definity, Bristol-Meyers Squibb Medical Imaging, Inc.) was administered as an i.v. bolus injection of 20 μL through a jugular vein puncture followed by a 20-μL saline flush. Single-slice B mode imaging was done (center frequency, 40 MHz; 50% power; axial resolution, 40 μm; lateral resolution, 100 μm; 20 frames per second). The ultrasound probe was aligned perpendicular to the animal and the tumor center was determined. Eight hundred frames were acquired for first-pass kinetics analysis, the first 20 of which were acquired before contrast agent injection. These processes were done in three planes (located within 1 mm of one another) and mean tumor area was calculated.

First-pass kinetics analysis of the signal intensity-time curve was used to measure relative blood volume (rBV) and vascular transit time for each pixel (19). Relative blood flow (rBF) was obtained for each pixel, where rBF = rBV/vascular transit time. A lower limit perfusion threshold was determined from regions within the tumor that showed no enhancement after contrast agent administration. Mean rBV, rBF, and vascular transit time were determined for the perfused tumor tissue. Mean tumor area was calculated as the average area in three tumor planes: the center and ±1 mm from the center of the tumor. Each tumor area measurement was calculated from an average of 15 B-mode (precontrast) frames acquired before injection of microbubbles. The averaging of the precontrast images provided a high SNR image. The border of the tumor area was traced to exclude the skin, subcutaneous fat and muscle.

Clinical study

Study design and patient selection. Ethical approval was obtained from the Local Research Ethics Committee. Regulatory approval was granted by the UK Medicines and Healthcare Products Regulatory Agency. Ten patients with liver metastases from histology-proven primary epithelial CRC and no previous cytotoxic chemotherapy exposure were recruited in an open label study. Written informed

consent was obtained. Patients ages ≥18 y, with an Eastern Cooperative Oncology Group score between 0 and 2, and life expectancy of at least 3 mo were eligible. All patients had at least one measurable lesion of ≥2 cm present on three or more adjacent MRI slices and had no previous treatment with VEGF inhibitors or cytotoxic chemotherapy, or contraindications to VEGF inhibitors.

Patients received single agent 10 mg/kg bevacizumab (cycle 1) followed every 2 wk by 10 mg/kg bevacizumab plus FOLFOX-6 (oxaloplatin/5-fluorouracil/leucovorin) for up to 6 mo (cycles 2-13). MRI scans were done during cycle 1 only, twice at baseline to establish parameter repeatability and then at 4 and 48 h posttreatment and days 8 and 12.

MRI data acquisition and analysis. Data were acquired on a 1.5T Philips Intera system (Philips Medical Systems). Anatomic precontrast T_1- and T_2-weighted images were done. Next, 75 axial T_1-weighted fast field echo volumes were consecutively-acquired every 4.97 s for a total of 6 min 13 s (*TR*, 4.0 ms; *TE*, 0.82 ms; $\alpha = 20°$; one signal average; FOV, 375 mm × 375 mm; matrix, 128 × 128, 25 slices) following calculation baseline of T_1 ($\alpha = 2°/10°/20°$; 4 signal averages; identical *TR*, *TE*, imaging matrix). Omniscan (0.1 mmol/kg; Amersham Health) was administered i.v. through a Spectris MR (Medrad, Inc) power injector at 3 m /s on the sixth dynamic time point. Slice thickness was 4 mm for small target lesions or 8 mm for larger lesions (superior-inferior coverage of 100 or 200 mm). Finally, a postcontrast T_1-weighted image was acquired.

Regions of interest were defined in three-dimensions on the spatially coregistered high resolution T_1- and T_2-weighted volumes to encompass the entire tumor of interest. Whole TV was measured for each lesion. Voxels whose precontrast and postcontrast agent time series had significantly different distributions (where $P < 0.05$ on Mann-Whitney Wilcoxon rank-sum test) were classified as enhancing. The enhancing fraction (E_F) was calculated by dividing the number of enhancing voxels by the total number of tumor voxels.

DCE-MRI data were analyzed using in-house software. Tumor T_1 was calculated using the known relationship between the spoiled gradient echo signal, *TR*, flip angle, and T_1. An arterial input function was measured where possible; alternatively, a population-derived function was applied (20) and the kinetic model parameters volume transfer constant (K^{trans}), fractional volume of the extravascular extracellular space (v_e), and fractional blood plasma volume (v_p) were derived using the extended Tofts version of the Kety model. The model free parameter initial area under the gadolinium contrast agent concentration time curve at 60 s ($IAUC_{60}$) was also calculated (21). All parameters were calculated voxel-by-voxel. Median values of T_1, K^{trans}, v_e, and $IAUC_{60}$ and the mean v_p were determined from the enhancing portion of each tumor regions of interest.

Statistical analysis

In the animal studies, statistical analysis was done with JMP statistical software package (SAS Institute, Inc.). Group comparisons for micro-CT and ultrasound metrics were evaluated with Student's *t* test. *P* values of <0.05 were considered significant.

In the clinical study, statistical analysis was done using R (version 2.7.0). DCE-MRI data were analyzed on the logarithmically transformed scale. Repeatability was assessed using the replicate measurements available at baseline across patients. Reductions relative to baseline were based on results from random effects models where lesion-to-lesion effects within patients were included as random effects; separate random effects models were fit for each time point during treatment (4, 48 h, 8, and 12 d). Antilogs of the mean differences between baseline and time points during treatment were calculated to obtain relative changes from geomean baseline values expressed as percentages. Due to the large number of parameters analyzed, *P* values of <0.01 were considered statistically significant. All *P* values are two tailed and were not formally adjusted for multiple comparisons.

Results

Ex vivo *evidence for rapid G6-31 antivascular effects.* Vascular density was measured using *ex vivo* micro-CT angiography along with corroborative histologic measurements. We found statistically significant reductions in vascular density following G6-31 treatment compared with control animals at both 24 h (G6-31 treated, 3.6 ± 0.6%; control, 7.7 ± 1.8%; $P = 0.005$) and 48 h (G6-31 treated, 3.2 ± 1.1%; control, 6.0 ± 1.9%; $P = 0.0005$; Fig. 1A). Three dimensional micro-CT renderings exhibited a greatest reduction in central (core) tumor vasculature and a more modest effect in the peripheral vessels, which include coopted host vasculature (Fig. 1B).

MECA-32 histologic analysis of the same animals confirmed significant reduction in vascular density to 40% to 50% of the levels observed in the control group at both 24 h (G6-31 treated, 1.8 ± 0.2%; control, 4.6 ± 1.9%; $P = 0.032$) and 48 h (G6-31 treated, 2.2 ± 0.7%; control, 4.3 ± 0.9%; $P = 0.00001$; Supplementary Figure and Fig. 1C). Vascular density estimates, measured by Micro-CT and MECA-32 staining, were not significantly different from the control group at 90 minutes after G6-31 administration.

In vivo *evidence for rapid G6-31 antivascular effects.* DCE-US studies were done with the same animal model to determine if the above results were detectable *in vivo*. Subsequent *ex vivo* micro-CT measurements were also obtained. No differences were found in ultrasound estimates of rBV and rBF, or the micro-CT measurement of vascular density obtained 4 h after G6-31 administration.

Tumor rBV was reduced in the G6-31–treated group relative to the control group at 48 h posttreatment (G6-31 treated,

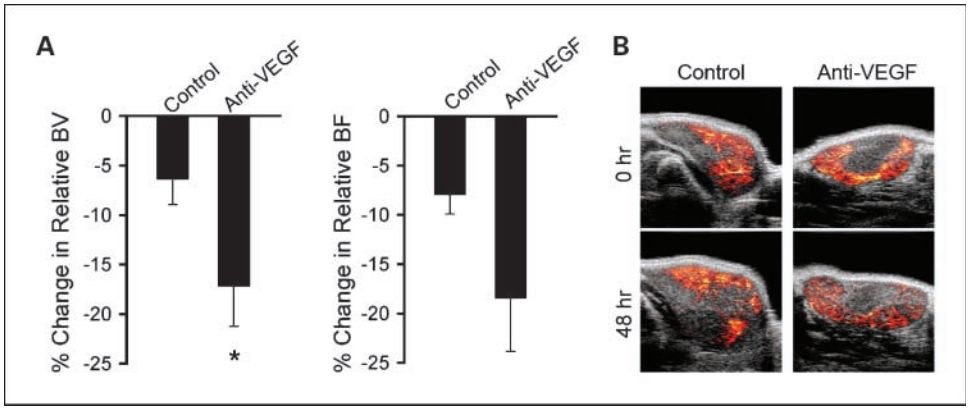

Fig. 2. *In vivo* evidence for reduction in rBV following G6-31. *A,* percentage change in rBV and rBF in control and treated groups after 48 h of anti-VEGF treatment. *B,* representative ultrasound perfusion blood volume maps for each treatment group pretreatment and at 48 h posttreatment.

Table 1. Percentage change in E_F, DCE-MRI parameters, longitudinal relaxation time, and whole TV measured from baseline to four posttreatment time points (4 and 48 h, and days 8 and 12)

Parameter	BL to 4 h		BL to 48 h		BL to day 8		BL to day 12	
	%	*P*	%	*P*	%	*P*	%	*P*
E_F	-7.5 -15.7 to 1.4	0.0913	-18.1 -27.9 to -7.1	0.0040	-22.2 -30.4 to -13.0	0.0005	-21.6 -32.1 to -9.6	0.0026
v_p	-34.9 -52.0 to -11.7	0.0086	-35.2 -59.5 to 3.6	0.0678	-40.9 -64.2 to -2.5	0.0410	-32.7 -46.7 to -15.0	0.0027
K^{trans}	-21.3 -30.8 to -10.5	0.0012	-25.5 -42.0 to -4.2	0.0243	-18.9 -32.0 to -3.0	0.0260	-9.0 -27.0 to 13.4	0.3719
v_e	-4.0 -16.3 to 10.1	0.5337	-5.9 -16.8 to 6.5	0.3132	-13.3 -26.2 to -1.9	0.0785	-6.8 -26.9 to 18.6	0.5393
T_1	-11.0 -18.7 to -2.6	0.0146	-0.3 -10.9 to 6.4	0.5374	-14.2 -23.5 to -3.9	0.0129	-18.1 -26.9 to -8.1	0.0023
WTV	-0.9 -8.9 to 7.8	0.8218	-0.8 -10.2 to 9.7	0.8704	-9.9 -27.1 to 11.3	0.3015	-14.5 -27.2 to 0.5	0.0569

NOTE: Mean values of percentage change and 95% confidence intervals are expressed. *P* values are two tailed, considered significant when <0.01, and were calculated using the mixed effects model on logarithmically transformed data.
Abbreviations: T_1, longitudinal relaxation time; WTV, whole TV; BL, baseline.

17.2 ± 9.9%; control, 6.3 ± 6.4%; $P = 0.048$). Tumor rBF exhibited a trend toward reduction in the G6-31–treated group at 48 h (G6-31 treated, 18.4 ± 13.3%; control, 7.9 ± 4.8%; $P = 0.0991$) that was not statistically significant (Fig. 2A). Micro-CT angiography analysis was done following animal sacrifice and showed significant reductions in vascular density for the G6-31–treated group relative to the control at 48 h ($P = 0.003$). Ultrasound rBV parametric maps for G6-31–treated tumors exhibited a heterogeneous spatial pattern consistent with the vessel loss observed in the micro-CT data (Fig. 2B, *bottom right*). These ultrasound data, along with the results from the micro-CT angiography time course study, show that a reduction in tumor rBV accompanies vessel loss following treatment with G6-31, suggesting that rBV is sensitive to structural change within tumor vasculature following antivascular therapy.

Mean tumor area was significantly increased in the control group compared with animals treated with G6-31 at both 4 h (G6-31 treated, 0.27 ± 4.7%; control, 5.1 ± 4.4%; $P = 0.0125$) and 48 h (G6-31 treated, 37.3 ± 11.6%; control, 70.4 ± 16.0%; $P = 0.00001$). These data suggest that structural changes in the tumor vasculature measured by endothelial cell staining, micro-CT, and ultrasound lead to rapid growth stabilization. The detection of tumor growth suppression at 4 h in the absence of statistically significant microvascular changes may reflect the limitations of micro-CT and ultrasound in detecting small vascular differences that were more pronounced at 24 to 48 h.

Clinical evidence for rapid antivascular effects induced by bevacizumab in human CRC metastases. Reductions in v_p and E_F were detected throughout the cycle of bevacizumab. In particular, statistically significant reductions in tumor E_F were measured at 48 h ($P = 0.004$) and maintained at days 8 ($P = 0.0005$) and 12 ($P = 0.0026$). These changes were accompanied by reductions in v_p at the corresponding time points (Table 1; Fig. 3). Representative parametric maps of enhancing voxels and v_p are shown (Fig. 4A and B).

Vascular changes detected in human tumors at 48 h concur with the above animal data. Rapid reductions in v_p indicate a loss of blood volume, consistent with the animal data detecting structural change in the tumor vasculature. In addition, the fraction of tumor that enhanced was significantly reduced (Table 1). A clear rim-core differential effect was observed as with the micro-CT data (Fig. 4A and B). These changes then persisted throughout the cycle of bevacizumab therapy, confirming that significant antivascular effects occur rapidly in humans and then persist following anti-VEGF monoclonal antibody therapy. These data provide evidence that v_p and E_F are sensitive to structural changes induced by antivascular therapy and are useful parameters for interpreting DCE imaging. Parameter within-subject coefficient of variation was 7.1% for E_F, 15.4% for K^{trans}, 48.1% for v_p, and 15.8% for T_1, showing comparable repeatability with the existing literature (22, 23).

In addition, we observed a statistically significant reduction of blood plasma volume 4 h after bevacizumab administration ($P = 0.0086$). This finding may represent a hyperacute hemodynamic response at 4 h in the human CRC metastases that differs from the sustained reduction (48 h through to day 12) in blood plasma volume that accompanied later vessel loss. A hyperacute response was not observed in the HM-7 xenograft studies. One possible explanation for the lack of a hyperacute hemodynamic response in the tumor xenograft model is that the HM-7 tumor vasculature is highly immature and lacks significant smooth muscle coverage.[9] I.v. dosing was used in these acute time point studies to maximize exposure over the short time period. It is unlikely that the negative results obtained at 90 minutes and 4 h could be due to the different route of administration because steady-state levels would be reached sooner with i.v. administration.

Bevacizumab induces change in K^{trans} and $IAUC_{60}$ in human CRC metastases. We found statistically significant decrease in median K^{trans} at 4 h ($P = 0.0012$) following bevacizumab therapy that remained suppressed to day 8. These reductions were not sustained at day 12 (Table 1; Figs. 3 and 4C), suggesting that K^{trans} is more sensitive to functional changes in the

[9] F.V. Peale, unpublished observations.

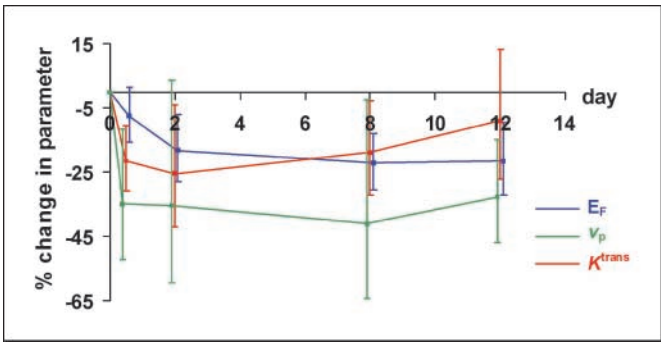

Fig. 3. *In vivo* evidence of the temporal evolution of antivascular effects of bevacizumab. Measurements of E_F, v_p, and K^{trans} in 26 tumors; bars, indicating the 95% confidence intervals for point estimates of log drops.

tumor vasculature rather than structural changes. Example parameter maps are shown in Fig. 4C. Change in median $IAUC_{60}$ mirrored those of K^{trans} (data not shown).

The timing and magnitude of these changes are in keeping with previous clinical trials of anti-VEGF antibodies (10) and TKI (12, 24, 25). However, changes in K^{trans} and $IAUC_{60}$ are difficult to interpret. $IAUC_{60}$ is relatively easy to calculate and repeatable but is not physiologically specific. K^{trans} is a composite estimate of both the blood flow and the permeability-surface area product per unit volume of tissue for transendothelial transport between plasma and extravascular space (26). The observed initial reductions in K^{trans} are, therefore, consistent both with an initial decrease in blood flow and/or a reduction in vessel permeability. This difficulty in interpretation is an important factor when the analysis of DCE imaging data are restricted to physiologically nonspecific parameters.

Evidence that bevacizumab induces edema resolution and tumor shrinkage. Reduction in TV was detected across the cohort of 26 tumors by day 12 (Fig. 5A), although this change did not reach statistical significance ($P = 0.0569$). No patients achieved partial response as defined by Response Evaluation Criteria in Solid Tumors. Based on the replicate observations taken at baseline, 95% of ratios of serial measurements of TV are estimated to be between 76.2% and 131.3%. Using these criteria, 9 of 26 tumors (in five different patients) exhibited statistically significant volume reduction (Fig. 5B).

Reductions in TV were accompanied by statistically significant reductions in tumor precontrast T_1 from baseline to day 12 ($P = 0.0023$; Figs. 4D and 5A), likely to represent resolution of tumor edema caused by reduced vascular permeability. This mirrors similar rapid resolution of edema observed following inhibition of VEGF with TKI AZD2171 in glioblastoma multiforme (27). Although a small cytotoxic effect secondary to the early antivascular effects of bevacizumab cannot be discounted, these data support the hypothesis that bevacizumab-induced reduction in vascular permeability and blood flow leads to reduced tumor tissue edema, accompanied by reduction in TV.

Discussion

Physiologic imaging can provide detailed quantitative information concerning tumor biology and drug mechanism of action that may help guide the rational development of targeted therapeutics (16). We have presented valuable new information concerning the temporal evolution of antivascular effects induced by anti-VEGF antibodies that has important implications for studies that evaluate antivascular or antiangiogenic agents.

Insight into drug mechanism of action. Previous studies have shown rapid reductions in vascular permeability. In one study, Berry et al. (28) found that 24 h after treatment with G6-31, K^{trans} was reduced 62% in the same HM-7 xenograft model that was used in this article. Our current results show that micro-CT angiography, a technique used previously to characterize normal tissue and tumor vasculature (18), can detect rapid vessel loss in murine HM-7 xenografts within the first 24 h following treatment with G6-31. This is the first study to show that an anti-VEGF therapy can reduce tumor vascular density within such a short time frame. These changes were accompanied by reductions in blood volume, observed at 48 h using DCE-US.

These data (measurements of blood volume and vascular density) reflect structural changes in tumor vasculature following anti-VEGF therapy and help interpret the clinical DCE-MRI data (measurements of fractional blood plasma volume and proportional tumor enhancement) at 48 h after bevacizumab administration in metastatic CRC. Further DCE-MRI data at 8 and 12 days provide evidence that these effects, likely to be structural, are maintained throughout a 2-week cycle of bevacizumab and lead to resolution of tumor edema and decrease in TV.

In distinction, the parameters K^{trans} and $IAUC_{60}$ showed transient reductions from baseline values that were lost by the end of the cycle of anti-VEGF therapy. Both K^{trans} and $IAUC_{60}$ reflect a combination of blood flow and capillary permeability, suggesting that these parameters are sensitive to transient functional changes in the tumor vasculature and that measurement timing is critical to detect these changes induced by anti-VEGF therapy.

Overall, these data provide evidence that the structural and functional changes induced by anti-VEGF monoclonal antibodies lead to rapid downstream effects in tumor morphology. Growth stabilization was shown within 48 h in murine HM-7 xenografts treated with G6-31, relative to controls. In the clinical data, CRC liver metastases showed statistically significant reduction in T_1, consistent with resolution in edema that was accompanied by a trend toward volume reduction across the group of metastases. In 9 of 26 lesions, the volume reduction was statistically significant. Taken together, these data provide cross-species evidence for antivascular effect with anti-VEGF antibodies within 48 h, with resultant rapid resolution of edema and tumor shrinkage.

There are several limitations to this study that qualify the above conclusions. For the preclinical study, a single xenograft model was evaluated by using multiple imaging modalities and time points. The extensive evaluation of a single responsive model does not provide a thorough evaluation of the magnitude of the vascular imaging response as a function of the responsiveness of the tumor. This would require the evaluation of number of additional models that represent a range (including a nonresponder) of responsiveness based on TV. This would likely provide additional insight into the range of the vascular response and answer the question of the state of these vascular imaging parameters in a nonresponding tumor. It would also be of value to evaluate a model of liver metastases, where

tumors would likely experience a more representative microenvironment to that experience by clinical CRC liver metastases. Although these are interesting questions, they are beyond the scope of this study, which focused on quantifying the vascular response of a tumor model where there is a potent anti-VEGF response as a means to better understand the vascular changes associated with the positive DCE-MRI response that has been observed in clinical anti-VEGF studies. For the clinical study, the temporal resolution of the DCE-MRI study was not sufficient to obtain independent estimates of blood flow and permeability.

Choice of physiologic imaging biomarkers in clinical trials. Traditional clinical trial assessment of tumor response has relied on codified radiological response criteria (29, 30). In Response Evaluation Criteria in Solid Tumors, a categorical measurement of treatment response is provided where *partial response* is defined as >30% reduction in the longest diameter of the sum of all marker lesions, which equates to around 65% reduction in TV (31). Using this approach, antivascular and antiangiogenic agents have been considered to induce insignificant changes in tumor size (8). This has stimulated considerable interest in the serial noninvasive evaluation of the tumor microenvironment in early-phase clinical trials of targeted therapeutics.

DCE-MRI and DCE-CT have been used to estimate tumor blood flow, blood volume, and edema and provide pharmacodynamic end points of drug activity in around 30 phase I/II clinical trials of anti-VEGF antibodies, TKI, and VDA. Nearly all of these studies have reported either K^{trans} or $IAUC_{60}$ as primary end points in line with consensus recommendations (32). However, these parameters have equivocal and complex physiologic meanings (9). This study shows the value of using multiparametric analyses that includes tumor T_1, E_F, and multiple modeled parameter end points that includes v_p, rather than K^{trans} and/or $IAUC_{60}$ alone. Such an approach enables changes in both the tumor vascular structure and function to be detected.

This study shows that measuring tumor size may yield important information in studies of some targeted therapeutic agents, when size change is assessed as a continuous (rather than categorical) variable. This finding concurs with previous reports in patients with metastatic renal cell cancer receiving sorafenib (33), suggesting that tumor size should remain an important metric for evaluating drugs that induce changes in blood flow and vascular permeability. In practice, it may be the combination of biomarkers based on tumor size, morphology, and function that provides the most useful evaluation of targeted therapeutics in early-phase clinical development.

Importance of measurement timing in image analysis. We have reported DCE-MRI data that quantify the temporal evolution of the antivascular effects of bevacizumab. To date, imaging studies have neither optimized scan timing nor had sufficient frequency of examination to accurately characterize the pharmacodynamic properties of novel therapies (9, 34).

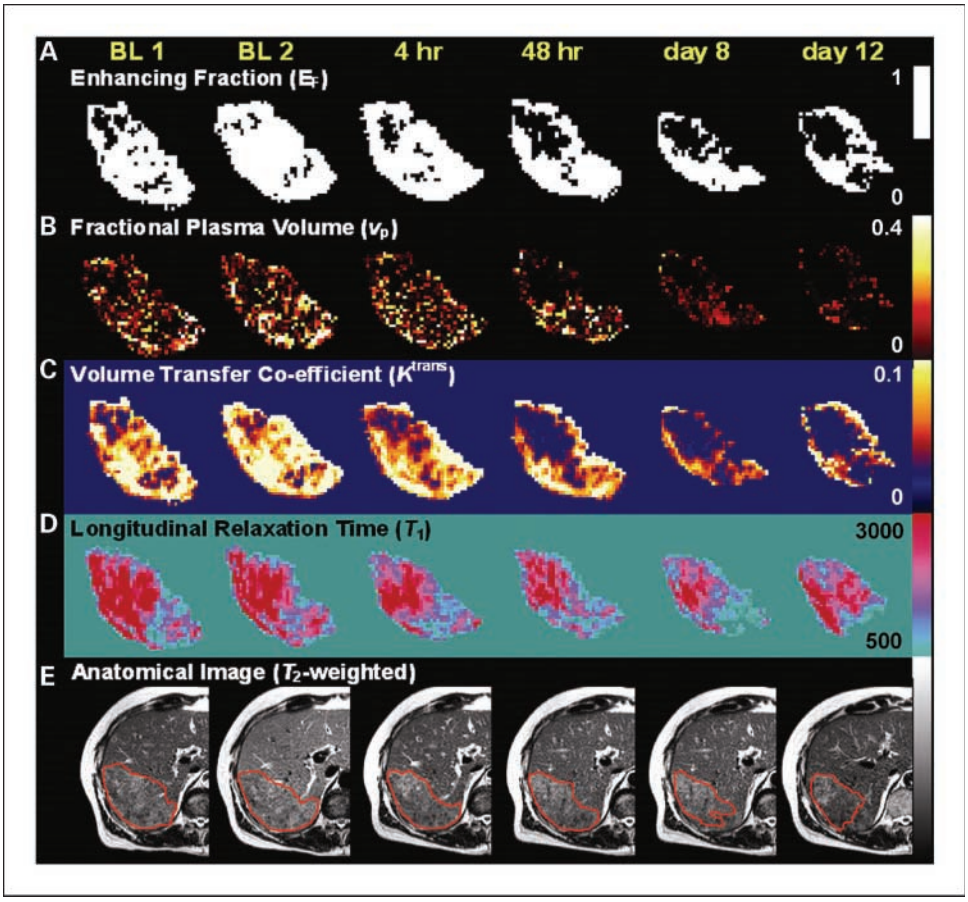

Fig. 4. Representative MRI parameter maps from one patient. *A,* map of enhancing voxels shows a significant decrease beginning at 48 h that persists through to day 12. Note that the loss of central enhancement. *B,* maps of fractional blood plasma volume (v_p) also shows a significant decrease, here beginning at 4 h that persists through to day 12. *C,* maps of the K^{trans} show reduction in parameter within 4 h that persist at 48 h and day 8, but return to baseline levels by day 12. These changes are consistent with reduction in either vessel permeability and/or blood flow. *D,* maps of the longitudinal relaxation time (T_1) measured before contrast agent administration show a clear progressive reduction in T_1, a parameter that can reflect changes in tumor edema. *E,* T_2-weighted anatomic image without contrast (arbitrary signal intensity units). All parameter maps and images were obtained at baseline twice (base 1 and 2) and at 4, 48 h, 8, and 12 d after bevacizumab administration. Tumors region of interest are outlined in red and show gradual reduction in tumor size.

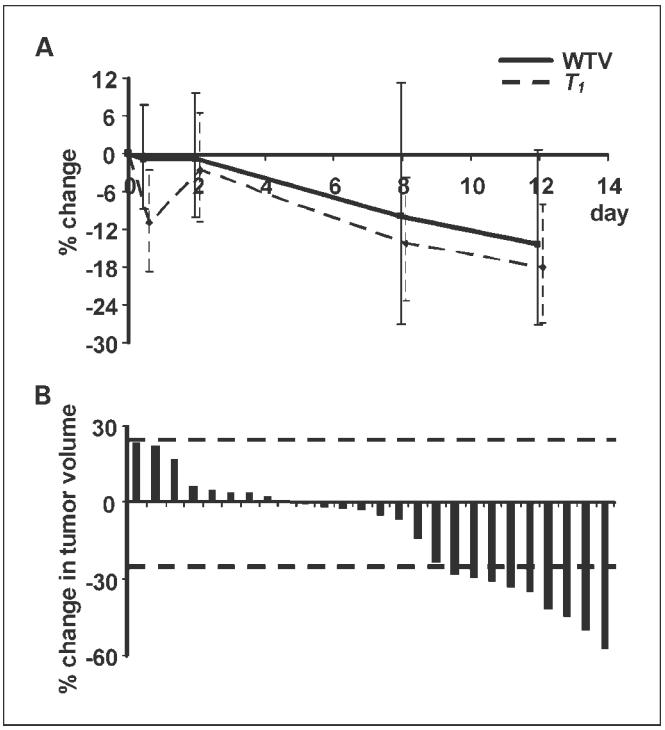

Fig. 5. Evidence for reduction in tumor size with bevacizumab monotherapy. *A,* temporal evolution of TV reduction and change in longitudinal relaxation time (T_1) from baseline through to day 12 in 26 tumors. *B,* waterfall plots show percentage reduction in TV from baseline size at day 12. *Dotted lines,* lesions that changed in size by greater than the lower and upper 95% confidence limits of serial parameter ratios.

Rapid anti-VEGF antibody-mediated antivascular effects have been reported in animal models (35), but the temporal evaluation of bevacizumab-induced antivascular effects in humans has not been done previously. In comparable studies, DCE-MRI measurements have been done at around 4 h postdosing to evaluate VDA (14) and around 24 to 48 h posttherapy to evaluate TKI (25, 27). Studies of bevacizumab have limited imaging end points to late time points in the treatment cycle; patients were imaged at 7 to 12 days following two weekly bevacizumab monotherapy in CRC assessed by DCE-CT (36) and at the end of a three week cycle in a DCE-MRI study of inflammatory breast cancer (11).

In this clinical study, we chose imaging time points at 4 and 48 h (consistent with the *ex vivo* and *in vivo* animal studies, and with trials of VDA and TKI) and day 12 (bevacizumab has been reported previously to impair blood flow and blood volume at this time in CRC; ref. 36). An additional time point was selected at day 8 because preclinical evidence has suggested that vascular normalization may occur within a week following administration of a VEGF receptor inhibitor (37). Our results show a complex temporal evolution of parameter change that underpins the interaction of tumor biology and drug mechanism of action and shows how pharmacodynamic biomarkers may be used to optimize evaluation of novel therapies (34). These results support the use of detailed physiologic imaging in small phase I/II studies of antivascular and antiangiogenic agents to define the optimum timing and frequency of image acquisition for large phase II and all phase III trials of the same agents, where practical and economical reasons limit the amount of imaging that may be incorporated.

Lack of validation is a major factor that limits wider acceptance and application of physiologic imaging such as DCE-MRI and DCE-CT to clinical studies of antivascular and antiangiogenic compounds. This study highlights the benefits of multimodality imaging in evaluating mechanism of drug action and how animal data using combined imaging and histology may help to interpret clinical imaging techniques. However, considerable further studies are required to validate the physiologic imaging biomarkers described in this study.

Disclosure of Potential Conflicts of Interest

R.A.D. Carano, J. Ross, C.C.K. Ho, F.V. Peale, M. Friesenhahn, H.B. Reslan, M.A.T. Go, G.J. Pacheco, X. Wu, T.C. Cao, S. Ross, N. Ferrara, and N. van Bruggen are all employees and stockholders with ownership interests in Genentech.

Acknowledgments

We thank Jeffrey Eastham-Anderson for developing the Metamorph algorithms, managing the histologic imaging, and automated image analysis of MECA-32–stained tumor samples, and Greg Plowman for his comments on the manuscript.

References

1. Senger DR, Galli SJ, Dvorak AM, et al. Tumor cells secrete a vascular permeability factor that promotes accumulation of ascites fluid. Science 1983;219:983–5.
2. Leung DW, Cachianes G, Kuang WJ, Goeddel DV, Ferrara N. Vascular endothelial growth factor is a secreted angiogenic mitogen. Science 1989;246:1306–9.
3. Ferrara N, Gerber HP, LeCouter J. The biology of VEGF and its receptors. Nat Med 2003;9:669–76.
4. Kerr DJ. Targeting angiogenesis in cancer: clinical development of bevacizumab. Nat Clin Pract Oncol 2004;1:39–43.
5. Hurwitz H, Fehrenbacher L, Novotny W, et al. Bevacizumab plus irinotecan, fluorouracil, and leucovorin for metastatic colorectal cancer. N Engl J Med 2004;350:2335–42.
6. Sandler A, Gray R, Perry MC, et al. Paclitaxel-carboplatin alone or with bevacizumab for non-small-cell lung cancer. N Engl J Med 2006;355:2542–50.
7. Miller K, Wang M, Gralow J, et al. Paclitaxel plus bevacizumab versus paclitaxel alone for metastatic breast cancer. N Engl J Med 2007;357:2666–76.
8. Ratain MJ, Eckhardt SG. Phase II studies of modern drugs directed against new targets: if you are fazed, too, then resist RECIST. J Clin Oncol 2004;22:4442–5.
9. O'Connor JP, Jackson A, Parker GJ, Jayson GC. DCE-MRI biomarkers in the clinical evaluation of antiangiogenic and vascular disrupting agents. Br J Cancer 2007;96:189–95.
10. Jayson GC, Zweit J, Jackson A, et al. Molecular imaging and biological evaluation of HuMV833 anti-VEGF antibody: implications for trial design of antiangiogenic antibodies. J Natl Cancer Inst 2002;94:1484–93.
11. Wedam SB, Low JA, Yang SX, et al. Antiangiogenic and antitumor effects of bevacizumab in patients with inflammatory and locally advanced breast cancer. J Clin Oncol 2006;24:769–77.
12. Drevs J, Siegert P, Medinger M, et al. Phase I clinical study of AZD2171, an oral vascular endothelial growth factor signaling inhibitor, in patients with advanced solid tumors. J Clin Oncol 2007;25:3045–54.
13. Hahn OM, Yang C, Medved M, et al. Dynamic contrast-enhanced magnetic resonance imaging pharmacodynamic biomarker study of sorafenib in metastatic renal carcinoma. J Clin Oncol 2008;26:4572–8.
14. Galbraith SM, Maxwell RJ, Lodge MA, et al. Combretastatin A4 phosphate has tumor antivascular activity in rat and man as demonstrated by dynamic magnetic resonance imaging. J Clin Oncol 2003;21:2831–42.
15. Workman P, Aboagye EO, Chung YL, et al. Minimally invasive pharmacokinetic and pharmacodynamic technologies in hypothesis-testing clinical trials of innovative therapies. J Natl Cancer Inst 2006;98:580–98.
16. O'Connor JP, Jackson A, Asselin MC, et al. Quantitative imaging biomarkers in the clinical development of targeted therapeutics: current

and future perspectives. Lancet Oncol 2008;9:766–76.

17. Liang WC, Wu X, Peale FV, et al. Cross-species vascular endothelial growth factor (VEGF)-blocking antibodies completely inhibit the growth of human tumor xenografts and measure the contribution of stromal VEGF. J Biol Chem 2006;281:951–61.

18. Shojaei F, Wu X, Zhong C, et al. Bv8 regulates myeloid-cell-dependent tumour angiogenesis. Nature 2007;450:825–31.

19. Schwarz KQ, Bezante GP, Chen X, Mottley JG, Schlief R. Volumetric arterial flow quantification using echo contrast. An *in vitro* comparison of three ultrasonic intensity methods: radio frequency, video and Doppler. Ultrasound Med Biol 1993;19:447–60.

20. Parker GJ, Roberts C, Macdonald A, et al. Experimentally-derived functional form for a population-averaged high-temporal-resolution arterial input function for dynamic contrast-enhanced MRI. Magn Reson Med 2006;56:993–1000.

21. Tofts PS. Modeling tracer kinetics in dynamic Gd-DTPA MR imaging. J Magn Reson Imaging 1997;7:91–101.

22. Jackson A, Jayson GC, Li KL, et al. Reproducibility of quantitative dynamic contrast-enhanced MRI in newly presenting glioma. Br J Radiol 2003;76:153–62.

23. Evelhoch JL, LoRusso PM, He Z, et al. Magnetic resonance imaging measurements of the response of murine and human tumors to the vascular-targeting agent ZD6126. Clin Cancer Res 2004;10:3650–7.

24. Morgan B, Thomas AL, Drevs J, et al. Dynamic contrast-enhanced magnetic resonance imaging as a biomarker for the pharmacological response of PTK787/ZK 222584, an inhibitor of the vascular endothelial growth factor receptor tyrosine kinases, in patients with advanced colorectal cancer and liver metastases: results from two phase I studies. J Clin Oncol 2003;21:3955–64.

25. Liu G, Rugo HS, Wilding G, et al. Dynamic contrast-enhanced magnetic resonance imaging as a pharmacodynamic measure of response after acute dosing of AG-013736, an oral angiogenesis inhibitor, in patients with advanced solid tumors: results from a phase I study. J Clin Oncol 2005;23:5464–73.

26. Tofts PS, Brix G, Buckley DL, et al. Estimating kinetic parameters from dynamic contrast-enhanced T(1)-weighted MRI of a diffusable tracer: standardized quantities and symbols. J Magn Reson Imaging 1999;10:223–32.

27. Batchelor TT, Sorensen AG, di Tomaso E, et al. AZD2171, a pan-VEGF receptor tyrosine kinase inhibitor, normalizes tumor vasculature and alleviates edema in glioblastoma patients. Cancer Cell 2007;11:83–95.

28. Berry LR, Barck KH, Go MA, et al. Quantification of viable tumor microvascular characteristics by multispectral analysis. Magn Reson Med 2008;60:64–72.

29. World Health Organization. WHO handbook for reporting results of cancer treatment. Geneva: World Health Organization; 1979.

30. Therasse P, Arbuck SG, Eisenhauer EA, et al. New guidelines to evaluate the response to treatment in solid tumors. European Organization for Research and Treatment of Cancer, National Cancer Institute of the United States, National Cancer Institute of Canada. J Natl Cancer Inst 2000;92:205–16.

31. Padhani AR, Ollivier L. The RECIST (Response Evaluation Criteria in Solid Tumors) criteria: implications for diagnostic radiologists. Br J Radiol 2001;74:983–6.

32. Leach MO, Brindle KM, Evelhoch JL, et al. The assessment of antiangiogenic and antivascular therapies in early-stage clinical trials using magnetic resonance imaging: issues and recommendations. Br J Cancer 2005;92:1599–610.

33. Karrison TG, Maitland ML, Stadler WM, Ratain MJ. Design of phase II cancer trials using a continuous endpoint of change in tumor size: application to a study of sorafenib and erlotinib in non small-cell lung cancer. J Natl Cancer Inst 2007;99:1455–61.

34. Jain RK, Duda DG, Willett CG, et al. Biomarkers of response and resistance to antiangiogenic therapy. Nat Rev Clin Oncol 2009;6:327–38.

35. Yuan F, Chen Y, Dellian M, et al. Time-dependent vascular regression and permeability changes in established human tumor xenografts induced by an anti-vascular endothelial growth factor/vascular permeability factor antibody. Proc Natl Acad Sci U S A 1996;93:14765–70.

36. Willett CG, Boucher Y, di Tomaso E, et al. Direct evidence that the VEGF-specific antibody bevacizumab has antivascular effects in human rectal cancer. Nat Med 2004;10:145–7.

37. Winkler F, Kozin SV, Tong RT, et al. Kinetics of vascular normalization by VEGFR2 blockade governs brain tumor response to radiation: role of oxygenation, angiopoietin-1, and matrix metalloproteinases. Cancer Cell 2004;6:553–63.